A Molecular Dynamics Study of the Laser Sintering Process and Subsequent Mechanical Properties of γ-TiAl Nanoparticles

Eleanor Dickens

Follow this and additional works at: https://egrove.olemiss.edu/hon_thesis

Part of the Other Mechanical Engineering Commons

A MOLECULAR DYNAMICS STUDY OF THE LASER SINTERING PROCESS AND
SUBSEQUENT MECHANICAL PROPERTIES OF γ-TiAl NANOPARTICLES

By

Eleanor Dickens

A thesis submitted to the faculty of The University of Mississippi in partial fulfillment of the
requirements of the Sally McDonnell Barksdale Honors College.

Oxford, MS

May 2022

Approved By

_____

Advisor: Dr. Shan Jiang

_____

Reader: Dr. Samrat Choudhury

_____

Reader: Dr. Yewei Han

DEDICATION

This thesis is dedicated to my friends, family and loved ones, especially my parents, who patiently encouraged me toward reaching my goals along my undergraduate path. I couldn't have done it without all their love and support. Thank you.

ACKNOWLEDGEMENTS

ABSTRACT

ELEANOR DICKENS: A Molecular Dynamics Study of Laser Sintering Process and Subsequent Mechanical Properties of γ-TiAl Nanoparticles

Using molecular dynamics (MD) simulations, the laser sintering additive manufacturing process is investigated through the observation of γ-TiAl nanoparticles. This process is conducted using both uni-directional chain and stacking configurations. By mimicking the heating process and varying laser sintering parameters such as heating rater, sintering temperature, and particle orientation, the fusion behavior and resulting products are analyzed for both chain and stacking NP patterns. In of single chain cases, it is noticed that slower heating rates and higher melting temperatures yield larger neck growth between each individual particle and thus produce a more stable product. This leads to stronger mechanical properties in subsequent tensile testing of the NP chain. In stacking configurations, it can be noticed that faster heating rates in stacking sequences yield for higher fusion temperatures which is contradictory to most past studies of the same nature using single chain patterns. Additionally, it is concluded that the closed pack ("Type C") stacking sequence also yields a higher melting temperature than the aligned pattern ("Type A") due to the increased number of neck connections and thus increased stability in the "Type C" NP stacks. Lastly in stacking patterns, it can be realized that varying particle orientation, while making a slight impact on in NP interaction in the melting process, yields no consistent trend, thus aligning with the random nature of particle orientation in real physical cases of NP laser sintering.

PREFACE

This thesis is a product of over three years of work that began in the winter of 2019. As the project was funded through a NASA grant, it sparked my interest as aerospace has been the field that I have had most inclement toward. I believe the work done through this research has been what has best suited me to start my career at NASA Marshall Space Flight Center. The work has pushed me to gain technical and logical experience that I would not have gained otherwise.

When I started running molecular dynamics simulations as a sophomore, I had very little knowledge on the subject. Thus, I cannot thank my advisors, Dr. Shan Jiang, and his graduate students Jungmin Jeon and Huadian Zhang enough for aiding me in my learning process. Molecular dynamics is a very unique and challenging field that I have gotten to spend time investigating and am so enthusiastic about devoting my Honors Thesis toward.

TABLE OF CONTENTS

LIST OF GRAPHS/TABLES

LIST OF ABBREVIATIONS

AM   Additive Manufacturing

SLS   Selective Laser Sintering

NP   Nanoparticle

MD   Molecular Dynamics

MSD   Mean Squared Displacement

CNA   Common Neighbor Analysis

FCC   Face Centered Cubic

BCC   Body Centered Cubic

HCP   Hexagonal Close Packed

INTRODUCTION

The development of additive manufacturing (AM) processes has shed more light on the study of nanoparticles for their improved nanoscale properties. AM processes such as selective laser sintering (SLS) lack research concerning the nanoparticle technology which could significantly contribute to higher quality in final manufactured products. SLS is one of the most rapidly growing means of prototyping techniques and desired for its wide abilities across different materials and applications. It requires the use of very fine powder to be heated by a laser and bonded into the shape of the product. The interaction between the laser and the powder is of crucial importance regarding the outcome of the final sintered product, [1]. Thus, this study designates focus toward the improvement of this process.
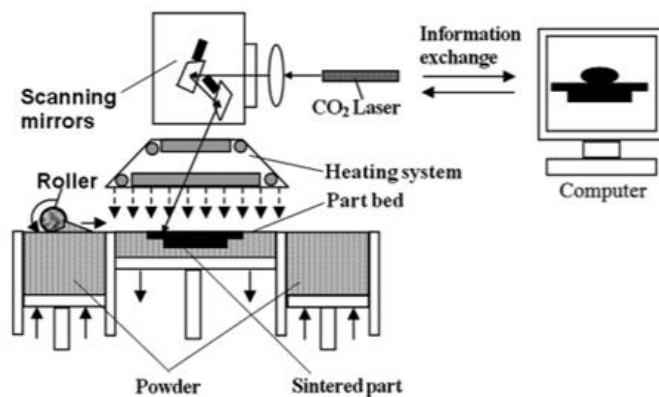
Figure 1: Schematic Illustration of the Selective Laser Sintering (SLS) Process

In the case of this study, laser remains the heat source while nanoparticles [NP] are the target material. Use of NPs are advantageous in the improvement of additive manufacturing technologies, as forms of this target material are varied by controlling their size and shape. These changes in the nanoparticle and heating process hold significant impacts on the outcome of the quality of the final sintered product. Changing the nanoparticle slightly can change its melting behavior abruptly due to the enhanced surface-to-volume ratio at the nanoscale [2]. Increasing research has gone into the variances of the laser heating processes and nanoparticle form to enhance knowledge at the ultra-fine nanoscale to obtain more optimal results at large.

Consequently, inclining interest has been contributed toward the use of molecular dynamics (MD) simulations to investigate the behavior of nanoparticles throughout and after the sintering process. MD simulations are preferred over continuum level as they reveal the unique property and behaviors of nanoparticles that continuum models are not able to reveal such as crystal orientations and neck formation between individual NPs [3].

MD simulations using γ-TiAl alloys are especially useful as these alloys are becoming more predominant in industry based on their high strength and capability of resisting oxidation at high temperatures. These characteristics are especially of interest in the aerospace and automotive industries where low weight and high temperature tolerance are usually necessary. Thus, the alloy draws interest in research efforts, especially in molecular dynamics simulations, to reveal more about its use from the nano scale to continuum level [4].

This specific investigation employs the use of bimetallic γ-TiAl nanoparticles in both single chain and 2-dimensional stacking sequences to investigate the effects of thermodynamic and tensile behavior from the SLS process. Similar studies have been conducted in different metals and alloys examining how factors in the NP chain such as particle type, size, and geometry effect

the final product. Additionally, factors such as heating rate and temperature of the laser sintering process are varied to observe its effect on the solidification and tensile results. This study, however, is unique as previous studies have studied either pure element or core-shell nanoparticles rather than bimetallic alloy particles. It is also unique in the fact that the simulations look beyond the behavior of just single chain particle formations but also NPs in stacking sequences. Specifically, this work will focus on the melting behavior of a single 5 NP chain of alloy particles by varying the melting rate and final melting temperature. A subsequent study is conducted to investigate how these properties effect the mechanical properties of the final product by applying uniaxial tension along the chain. In the NP stacking cases, effects of heating rate on the melting process will likewise be analyzed in addition to the effect of the variation of the form of stacking sequence and individual particle orientation.

PART 1: SIMULATION METHODOLOGY

Molecular Dynamics (MD) simulations are performed using large-scale atomic massively parallel simulator (LAMMPS). For both studies in single chain and stacking sequences, the configurations are made using the open-source software ATOMSK before simulating in LAMMPS. The software allows the user to use a variety of materials in bulk and utilize specified commands to obtain the desired particle configuration. To account for forces due to atomic interaction, the embedded atom method (EAM) forcefield was employed throughout. EAM is based off a quasi-atomic concept where the nuclei of colliding atoms overlap to appear as a single atom. The energy in the entire simulation box due to these forces is expressed as:

$$\textbf{Equation 1}: E_{total} = \sum_i F_i \rho_i$$

where F_i is the embedded and ρ_i is the density of the background.

Once adequately assembled into either their respective chain or stack configuration, the NP patterns step through a process of solid-state sintering, laser sintering, equilibrium, solidification and in the case of the single NP chain simulations, tensile testing. Each simulation done in LAMMPS on the single nanoparticle configuration and the stack were performed at 0 pressure with a 0.002 ps. timestep. The system's thermal properties are computed every 100 steps during the processes of heating and cooling. From each solid sintering, heating, cooling, equilibrium, process, there are a set of output values that are indicative of the different responses.

For both cases of single chain NPs and NPs in stacking sequences, one of the main indicators of the configurations condition during the sintering processes is the output of the mean squared displacement (MSD). MSD calculates the average distance a particle travels throughout simulation. This is especially of interest when evaluating melting behavior as particles move inward, or coalesce, toward one another during the fusion process. Thus, MSD is a good indicator of sintering melting temperatures between the different configurations. This value is calculated in LAMMPS by using the equation:

$$\textbf{Equation 2: } MSD = \left(\frac{1}{N}\right) \sum_{i=1}^{N} [r_i(t) - r_i(0)]^2$$

Here, N is the total number of atoms, t is the time instant, and r is the current position of each individual atom. For this study, MSD is calculated using the initial atom coordinates at the start of each simulation [5].

Another useful calculation computed in each of the LAMMPS sintering scripts is the of radius of gyration (R_g^2). It is the mean squared distance of a group of atoms as measured from the center of mass. This value is even more essential in the representing of the shrinkage in both the NP chain and sequence sintering simulations. It is shown by the equation:

$$\textbf{Equation 3:} R_g^2 = \frac{1}{M} \sum_{i=1}^{N} m_i (r_i - r_{cm})^2$$

where M is the group's total mass, r is the position of each individual atom, r_{cm} is the position of the center of mass, and i accounts for over all atoms in the group. Not only does this output reveal the shrinkage of each configuration, but also is indicative of the neck growth between neighboring NPs.

Additionally, atomic configurations were viewed throughout the duration of simulation using OVITO imaging software to further investigate sequence form, phase changes, and perform common neighbor analysis (CNA). This method of analysis allows for the further observation of phase change and crystal defect, especially in neck connections.

CNA is defined as the decomposition of the radial distribution function between atom pairs which provides the interpretation of various features with respect to its radial distribution in terms of atomic structure. This tool can be used to provide interpretation of such as stacking faults and changes in crystal structure. In the case of MD sintering studies, CNA can be used to observe the evolution of crystal structure throughout solid sintering and heating. OVITO will identify each as either BCC, FCC, HCP or disordered. Initially, γ-TiAl holds a face centered cubic (FCC) crystal structure with a lattice parameter of 4.11 Å Identifying of the crystal structure present in the simulation is reliant upon the correct use of the cut off distance (r_i) of atoms with respect to one another [6]. Cutoff distance for FCC particles is calculated by the following equation:

$$\textbf{Equation 4: } r_c^{fcc} = \frac{1}{2}\left(\left(\frac{\sqrt{2}}{2} + 1\right)a \cong 0.8536\right.$$

Where *a* is the lattice parameter for the respective material's structure. Thus, by correctly identifying this value in the OVITO, the imaging software can visualize the crystal structure evolution by accounting for the microstructure changes of the particles with respect to their distance with one another [7].

Information on Single Chain Simulations

In the case of the single chain 5 nanoparticle simulations, a single FCC γ-TiAl crystal was multiplied to make a bulk pattern. From bulk, a sphere with a 10 nm (100 Å) radius is cut with the surrounding particles outside of this radius reduced from the model. The initial single spherical particle is equilibrated before multiplying into its chain configuration. The particle is equilibrated at room temperature (298 K) using an NVT ensemble with a fixed temperature for a duration of 100 ps. Once the single NP is adequately equilibrated; the model is multiplied into its 5 NP chain configuration spanning in the x- direction with a 4Å spacing between the outer diameter of each NP. To mimic an infinitely long chain, eliminating length restraints on the simulation, a periodic boundary is employed only in the x-direction. Periodic boundaries are not employed in both the y and z direction to restrict the size of the simulation in these directions that are less of interest. Once the 5 NP chain is fully assembled, another NVT equilibration is enacted on the model for 100 ps at room temperature (298 K).
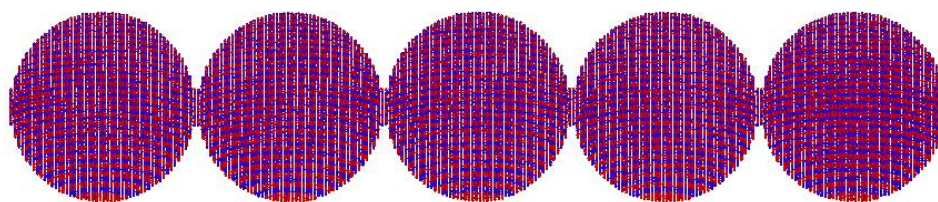
Figure 2: γ-TiAl Alloy- 5 NP Stack Structure

Once the NP chain is properly equilibrated and assembled, the single chain undergoes processes to closely mirror selective laser sintering conditions. To achieve such conditions, the chain undergoes the heating process using an NPT ensemble (fixed temperature, fixed pressure). To investigate the effect of sintering temperature, chains are heated up to four different final heating temperatures: 800K, 1200K, and 1500K. The temperatures are achieved using heating rates of 0.04 K/ps and 0.2 K/ps to observe the effect of heating process variation on the final

sintered product. This process required the use of a recentering command which constrains the center of mass by adjusting particle coordinates throughout each timestep. This command is set to restrain the center to its initial value at the beginning of the run.

Once the NP chain is heated up to its final respective temperature, it is cooled using the same boundary conditions as seen in the heating process but in reverse using a 0.08 K/ps cooling rate back down to 298K. The relatively slow cooling rate is chosen to try to mimic cooling in ambient environment after ultrafast heating. When the NP chain is brought back to room temperature, it undergoes another 1ns of equilibration to release any remaining stresses present from the dynamic cooling process.

A variation of tension simulations is then performed on the NP chains to investigate its mechanical properties after going through the selective laser sintering process. After arriving at a final and stable sintered product, the chain is subjected to uniaxial tension tests with a strain rate of 0.1 %/ps along the x-axis. This strain rate is computed as

$$\textbf{Equation 5}: \dot{\varepsilon}_{xx} = \frac{\Delta \varepsilon_{xx}}{\Delta t}$$

Here $\varepsilon_{xx} = \frac{\Delta \varepsilon_{xx}}{\Delta t}$ expresses the normal strain at each time step in the chain, ΔL_x is the change in length from the original length where L_x is the original length of the simulation box. Strain outputs are plotted against the stress values which are computed using the virial theorem [5]. Results of the subsequent mechanical processes are calculated using the stress values from these tensile processes. These values are output in LAMMPS and compared for each product sintered at different temperatures and heating rates. The tensile processes are animated and observed in OVITO to observe each trend.

Stacking Sequence Simulations:

To construct the stacking structure for simulations, single nanoparticles of 25 Å radii were cut from bulk using ATOMSK opensource software. Before construction into the multiparticle stacking model seen across simulations, the cut particle is equilibrated using a Nose Hoover thermostat (NVT) ensemble where temperature is fixed at 298K. The initial velocities are assigned to the particle at this temperature using a Gaussian distribution. The single NP configuration utilized a large simulation box to eliminate the possible allowance of any external disturbance.

2Å
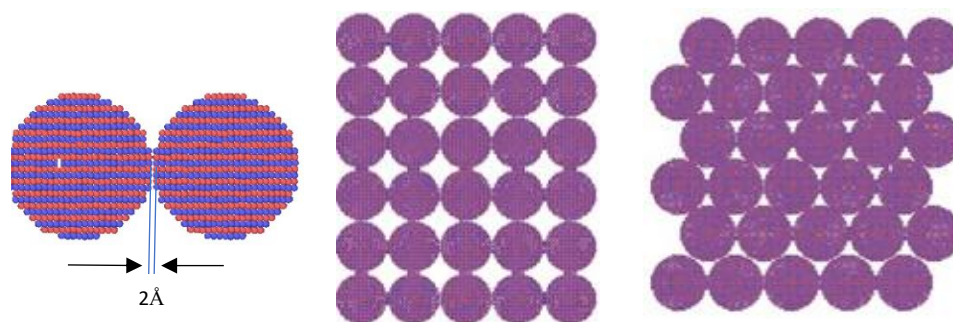
Figure 3: a.) Demonstration of Neighboring NP- spacing in between b.) "Type A" NP Stacking Sequence-Aligned c.) "Type C" NP Stacking Sequence- Closed Packed

When the single nanoparticle configurations had undergone correct construction, two different stacking models were made to create methods with different numbers of sintered necks. The "A" (aligned) stacking pattern features a normal NP stacking alignment method with particles stacked directly on top of one another creating a grid mesh pattern. The "C" (close packed) stacking pattern is a sequence that alters the normal A stacking sequence by moving alternating rows of NPs by a half diameter. In both cases, the particles are separated by a 2Å space between.

The type C stacking sequence entails that each particle will share 6 neck interfaces with its neighboring particle as opposed to only 4 necks in the type A pattern. This difference results in more free space exposure interface in type A molecules.

To observe the effect of particle position within the stacking sequence, the orientation of the particles is varied. Different particle orientations are investigated because in physical applications of NP materials, single particles are randomly distributed. With random orientation there are different ways in which the surfaces of the particles line up with each other when considering the layer structure of γ-TiAl. Though not oriented in a random manner in this study, varying the orientation reveals how the plane orientation of NP connection effects the heating process of NP configurations. The three orientations investigated in these simulations are its original normal orientation, rotated at 45° clockwise, and rotated 90° clockwise from its original position.

Also investigated is the effect that laser heating rate has on the melting behavior of the sintering process. Each stacking sequence is heated at a linear, fixed rate of 0.2 K/ps and 0.5 K/ps. All simulations are run to 1700K to heat particle set up to its melting point, and therefore invoke a phase change from its original solid state.

The simulation's output yield results that identify the thermal properties of MSD and relative radius of gyration to investigate the configuration change of stacked NPs throughout the sintering process. From viewing these properties, it is possible to investigate how properties such as melting point and neck connections are affected. Throughout the heating process, OVITO imaging software is used to periodically illustrate the changes seen in the sintering processes. Likewise, from the view of the common neighbor analysis, the change in crystal structure is analyzed to view any significant changes within the NP makeup.

PART 2: 5 NP SINGLE CHAIN RESULTS- LASER SINTERING PROCESS AND

UNIAXIAL TENSION APPLICATION

Laser Sintering Process Observations

      In the case of the single chain simulations, the main area of observation is the effect of

heating rate and final sintering temperature of the final product. Thus, for the *γ-TiAl 5 NP* chain,

the configurations are each heated to varying sintering temperatures of 800K,1200K and 1500K

at two different heating rates of 0.04 K/ps and ultrafast 0.2 K/ps. Before the NP chains undergo

heating processes, neck connections and growth are observed in the initial solid state sintering

equilibration. In this stage, individual NPs will directly contact adjacent neighbors automatically

due to their fine sized and large potential gradients between particles [8,9]. The crystal structure

for the NP chains after this process is shown in figure 4 below along with crystal structures

throughout the whole process of this study.

    After the solid sintering state, simulations mimicking the conditions of typical laser sintering

are carried out for the various sintering temperatures and heating rates. To characterize the

sintering process, mean squared displacement (MSD) and radius of gyration (R_g^2) calculations

are observed. MSD values are calculated using trajectory data that provides measures of atomic

distances during sintering. Additionally, these results aid in the investigation of the role that final

sintering temperature makes on the sintered product as well as the identification of disordered

atoms from high heating levels. Its R_g^2 values indicate the shrinkage of the chain by using a

relative value to the initial state to yield a percentage of shrinkage.

MSD for the various heating processes is shown in figure 5 displaying the effect of final sintering temperature and heating rate on the final chain product.
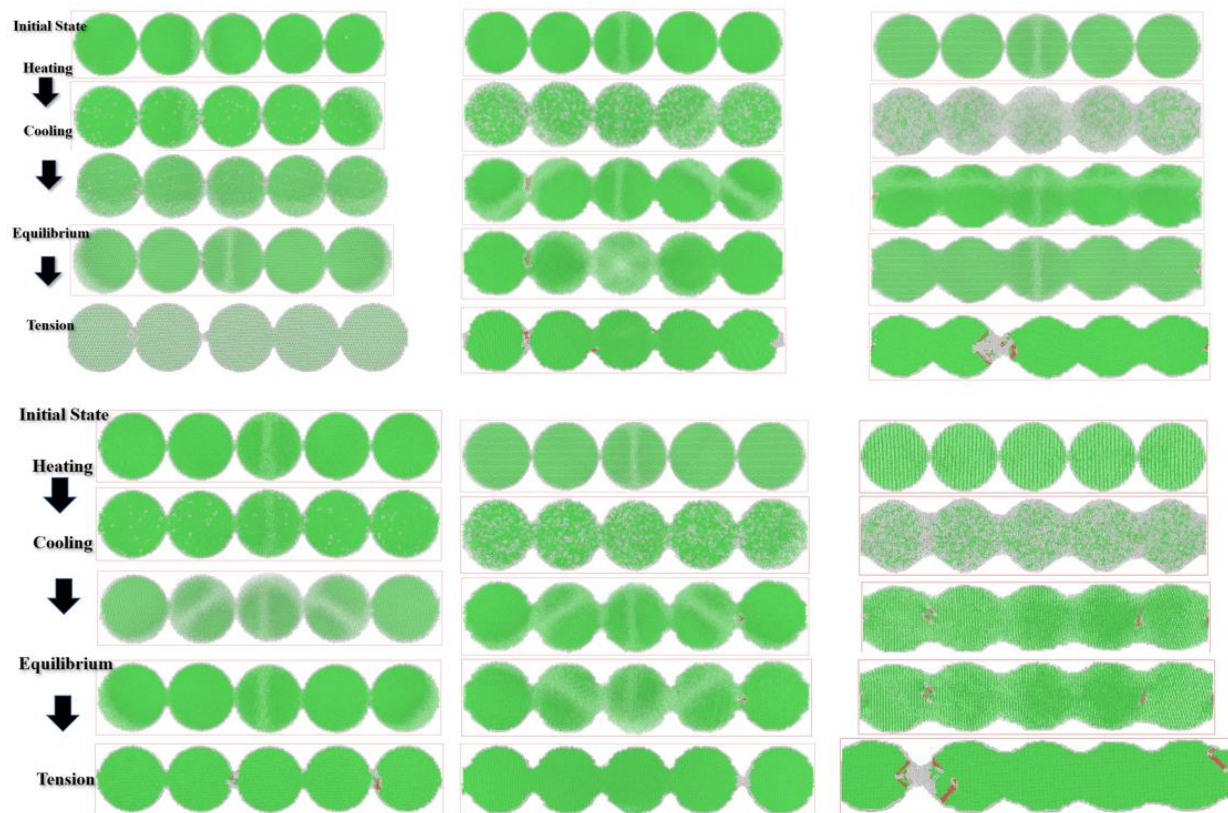
Figure 4*: Simulation Process for Various Sintering Heating Rates and Temperatures: a.) 0.04K/ps-800K b.) 0.04 K/ps-1200K c.) 0.04 K/ps-1500K d.) 0.2 K/ps-800K e.) 0.2 K/ps-1200K f.) 0.2 K/ps-1500K*

The results show sintering cases at a 0.04 K/ps and 0.2 K/ps heating rate to temperatures 800K, 1200K and 1500K. With the same heating rate, it is expected that the sintering process are to show similar MSD and gyration radius trends. As seen from the graph, in the case of the slower heating rate, the MSD shows oscillation from its original position and maximum value. This effect is more prominent as the temperature is risen throughout cases. In the case of the ultra-fast 0.2 K/ps heating rate, the oscillating effect on the MSD values is less prominent, however, the trend is noticed to start in the highest temperature case of 1500K. However, this

phenomenon is not nominal when compared to other similar cases such as in Zhang et al (2021) [10].
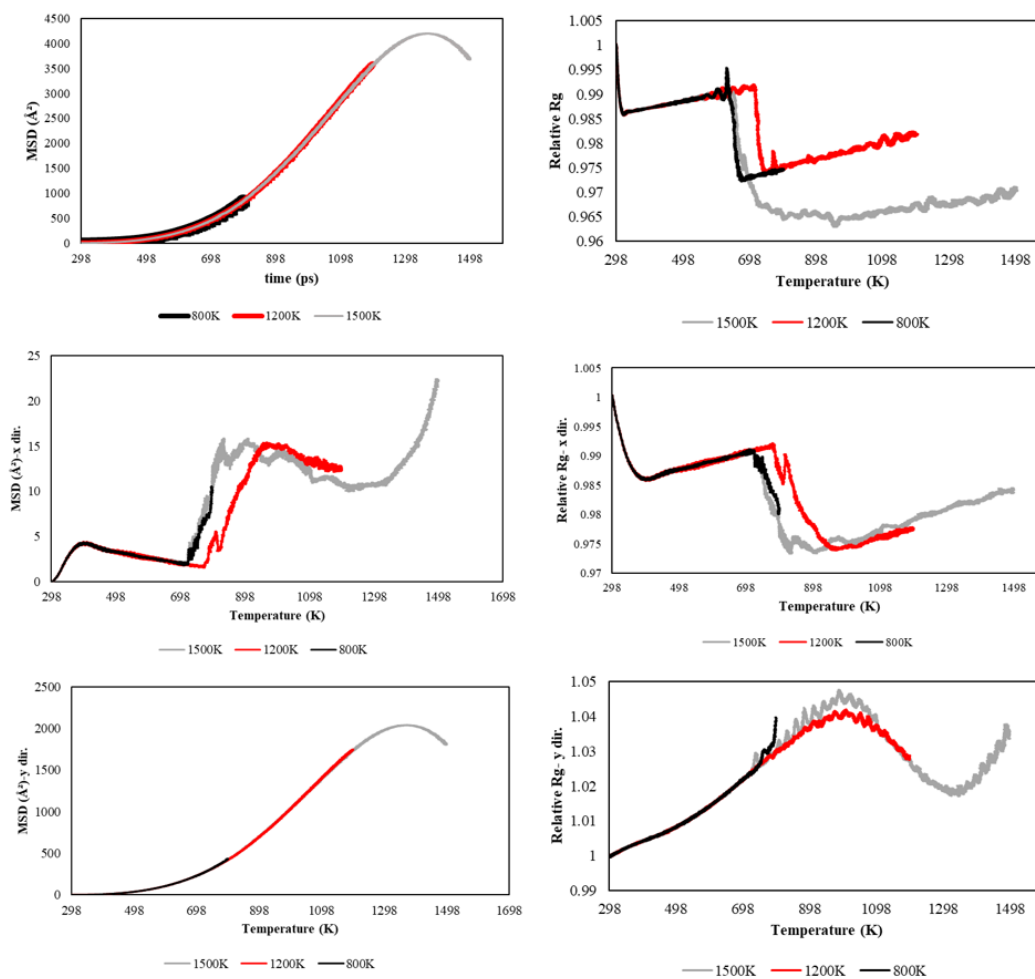
Figure 5: MSD & Rg Results for 0.2 K/ps Heating Rate- Magnitude and Directional Components
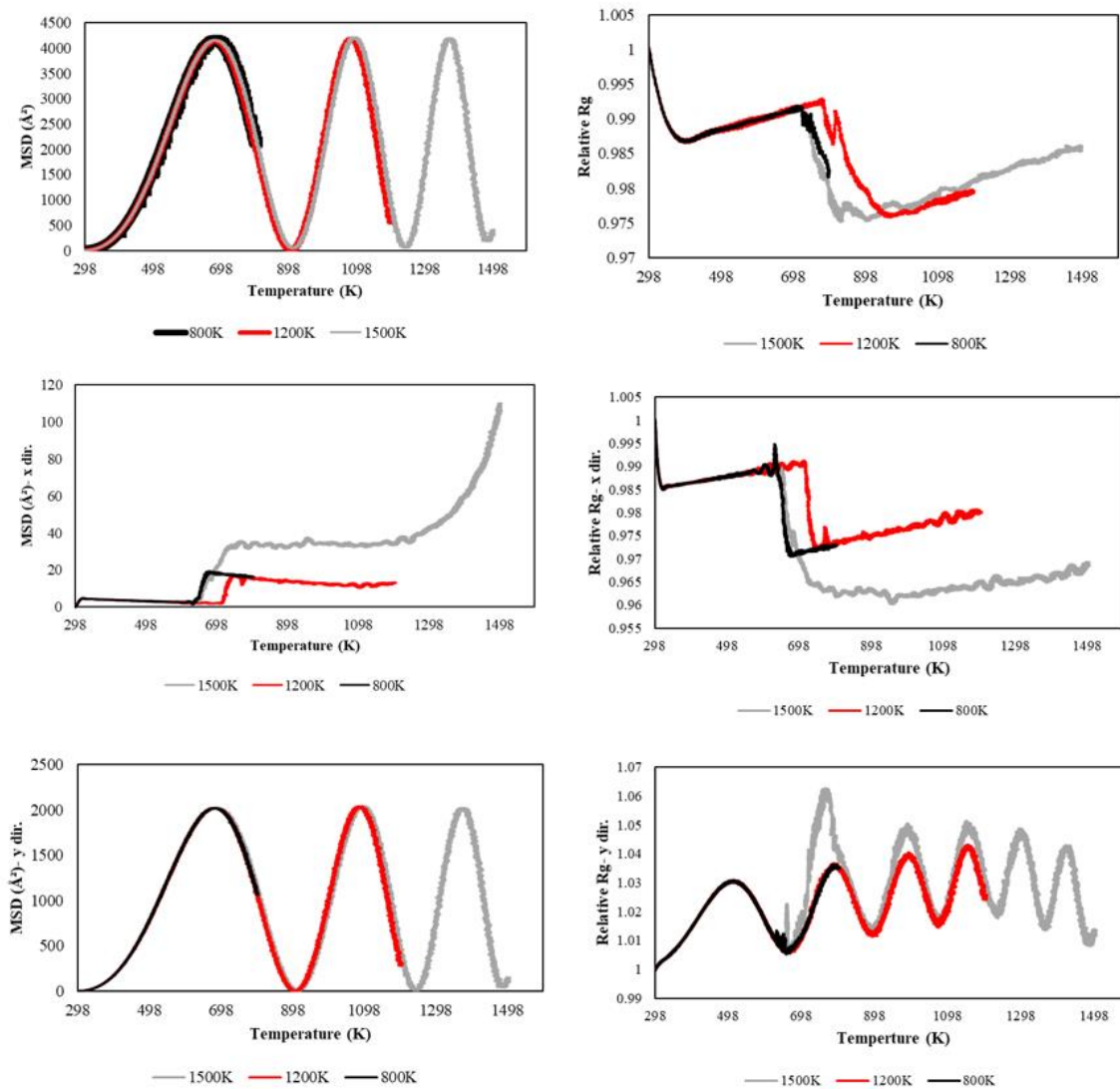
Figure 6: MSD & Rg Results for 0.04 K/ps.- Magnitude and Directional Components
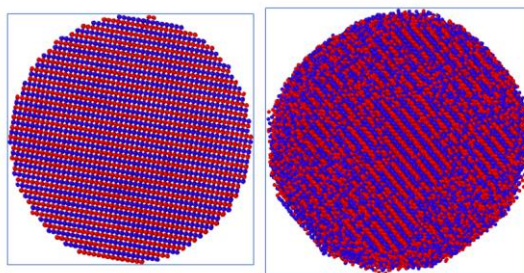
Figure 7: Demonstration of expansion in y-direction for Single stack Configuration

Originally, this trend was thought to be erroneous, as such oscillation MSD is physically inexplicable. However, by separating the R_g and MSD results into directional components and reobserving the process images in from different orientations, it was seen that the respective plots were a result of increased expansion in the y and z direction while coalescing occurs in the x direction. This is physically feasible as shrinkage in one direction typically leads to expansion in another in terms of size and movement. Thus, the magnitude of MSD in all directions is mainly driven by movement in the y and z directions, which is not of primary interest but still considered in the numerical output of the simulations. It is more telling to observe the trends in the x-direction. While logical, this output is still off nominal in terms of the values seen for the magnitude of MSD. Thus, future investigations will be necessary to correct this phenomenon in simulation output.

From viewing the plots in the x-direction for MSD, it is observed that there are portions of sharp increase and constant slope increase of less magnitude. The points of sharp increase are fusion points where the particles begin to coalesce with one another which is a characteristic part of the melting process. The portions of stable increase are indicative of stable neck growth phases between individual NP as they interact with one another in the melting process. In the case of gyration radii, these portions are decreasing instead of increasing, but distinguish the same trend. For the case of the slower 0.04 K/ps heating rate, values for MSD are higher while relative gyration radius shows a more drastic decrease throughout the cycle from its original size. This indicates that the slower heating rate yields a thoroughly sintered product with more stable neck growth between each particle as there is more time allowed for sintering.

After the melting process, a relatively slow cooling process takes place to demonstrate the solidification of nanoparticles after phase change in melting. This solidification process takes

place at a constant, linear -0.08 K/ps cooling rate. This relatively slow heating rate mimics the final product of ultrafast laser sintering, especially seen at the 0.2 K/ps heating rate, then being exposed to ambient conditions until reaching room temperature. Though variance in cooling rates could have a direct impact on the final NP product, its effect was not observed during this study as heating rate was the focus. Across all cases the main changes that occur in the cooling process is in the crystal structure especially in the case of elevated heating rates. When temperatures are elevated closer to the point of melting, the crystal structures changes as the particles approach phase change. Upon solidification in, the nanoparticles begin to regain their original structure.

For each sintering variation, visuals for significant points in the process are shown in figure 4 using OVITO imaging software. Since high sintering temperatures up to 1200K and 1500K are reached, larger discrepancies between the neck widths will be observed in varying sintering methods at different heating rates. As confirmed in the work by Zhang et al. (2021), largest, and thus strongest, neck connections are associated with the sintered products heated to highest temperatures with slow heating rates of 0.04 K/ps [10]. This can be explained by the fact that such configurations with slow heating allow the most sintering time for coalescence and form stronger bonds in the interface of individual atoms. Higher heating temperatures encourage greater coalescence between nanoparticles as they near melting temperature, thus also leading to larger neck connections.

Subsequent Uniaxial Tension Application Observations and Results

After the sintering, cooling and equilibration processes were completed, tensile processes were carried out with an applied strain rate of $0.1 \ s^{-1}$. The study was initially intended to additionally investigate the effects of varying strain rates with using 0.01 and ultra-slow

$0.001 s^{-1}$, however, due to inaccuracies in the yield point within the neck of the particles and the very large computation time required, these simulations will be left for future work. Thus, the main concern is to investigate the roll that final sintering temperature and rate will have on the tensile strength of the resulting nanoparticle chain product.
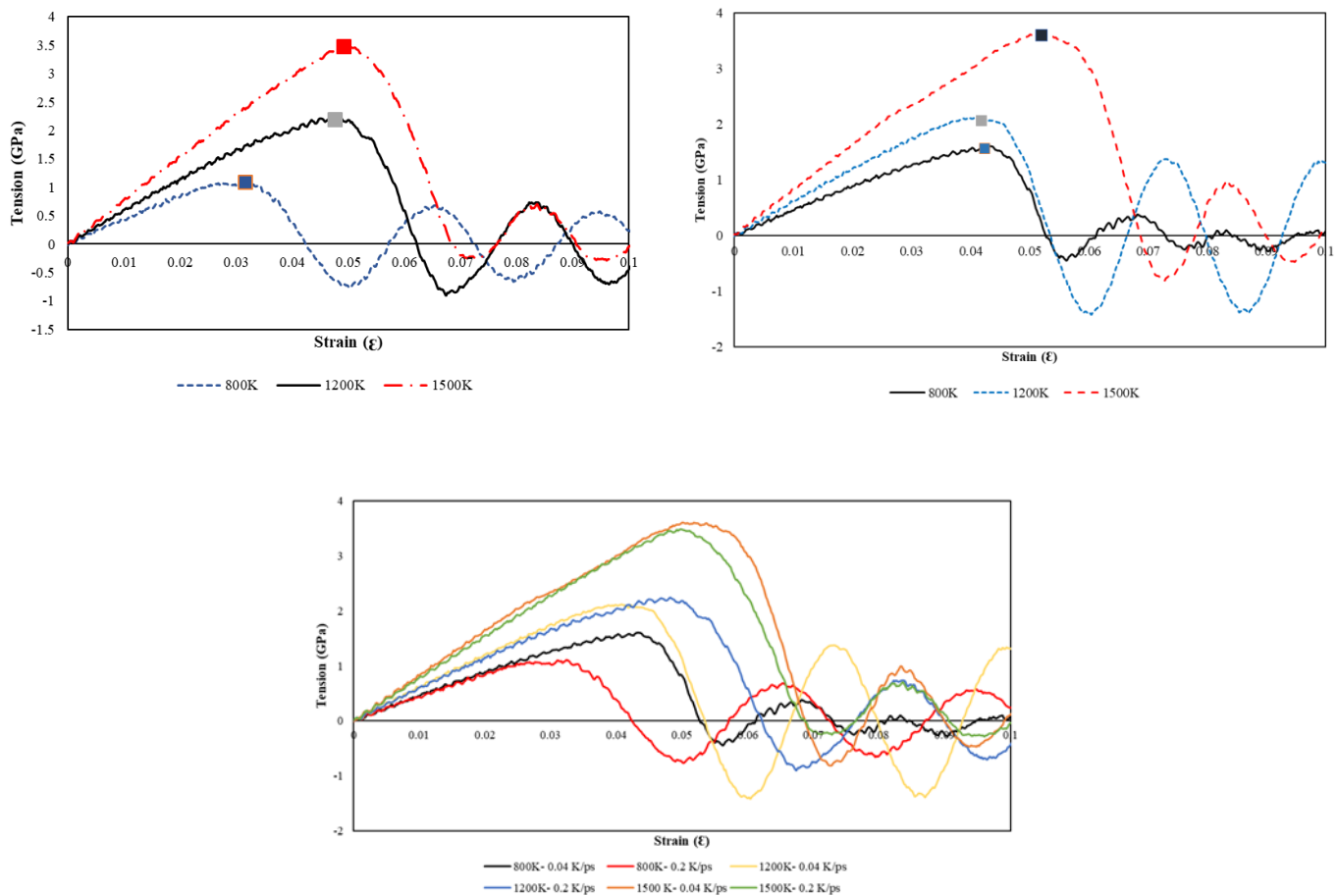
Figure 8: a.) 0.2 K/ps HR Cases Tensile Testing b.) 0.04K/ps HR Cases Tensile Tesing c.) Combined Tensile Testing- All Cases

The tension plots are shown for both 0.2 K/ps and 0.04 K/ps heating rates with varying temperatures as well as all the cases combined. As seen across plots, tensile strength increases with sintering temperature. Additionally, it is seen that ductility also increases with the increase in melting temperature. This is because increased melting temperature allows the creation of

larger, and thus stronger, necks between each individual nanoparticle as the increased

temperature causes particles to coalesce more readily. This is the case for both heating rates. By

viewing the combined tension cases of all temperature and heating rates of interest, it is seen that

using a slower sintering rate generally increases tensile strength and ductility. This is because

using a slower sintering rate requires more sintering time for the NPs to reach target temperature.

The increased time results in more thorough sintering between NPs with larger and more stable

neck connections. With stronger bonds between individual particles in the formation of bonded

necks, slow heating rates and high melting temperatures present the strongest final product in

tension. These results are confirmed in the work of Jeon et al [2019][5].

PART 3: NANOPARTICLE STACKING SEQUENCES: OBSERVING HOW HEATING RATE, SEQUENCE TYPE AND PARTICLE ORIENTATION EFFECT THE SINTERING PROCESS

Solid Sintering Process

As stated previously, both "A" and "C" type stacking sequences were sintered at room temperature (298 K) for 1 ns (1000 ps). This causes an excitation between solid state atomic forces that relieves any initial stresses. The MSD and relative radius of gyration (R_g) *(Fg. 8 a-b)* are recorded to analyze the shrinkage and change of particle density in the stacking sequence of interest.
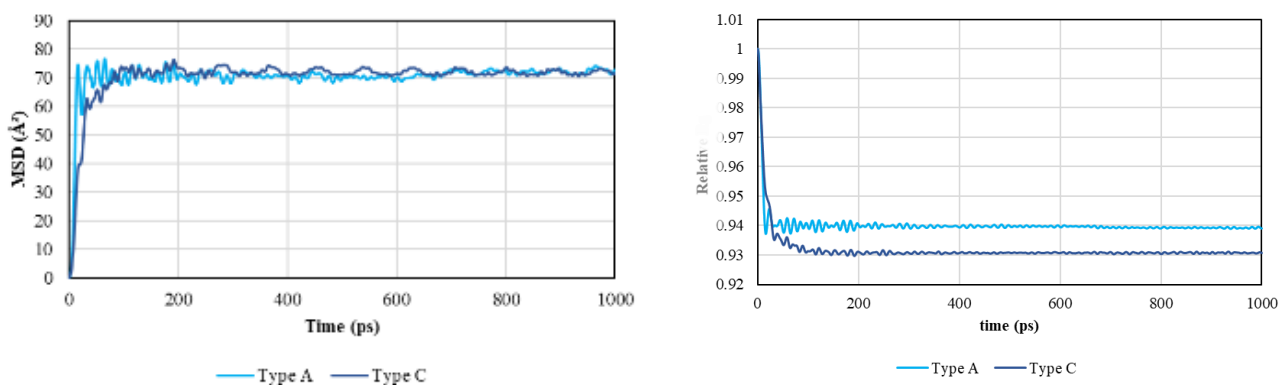
Figure 9: a.) MSD Results for Type "A" and "C" Solid Sintering b.) Gyration Radius Results for Type "A" and "C"

From the following plots, it can be observed that "type C" molecules have a slightly lower MSD and more drastic drop in their relative radius of gyration. This is due to the fact that the "C" sequence pattern starts with a higher initial particle density, in other words, are more closely assembled in the simulation box. From the trend, it can be assumed that a larger initial atom density yields a smaller increase in MSD value upon solid state sintering.

To illustrate the process, initial and final stages are shown for Type "A" and "C" particles during the solid sintering processes in figure 7.
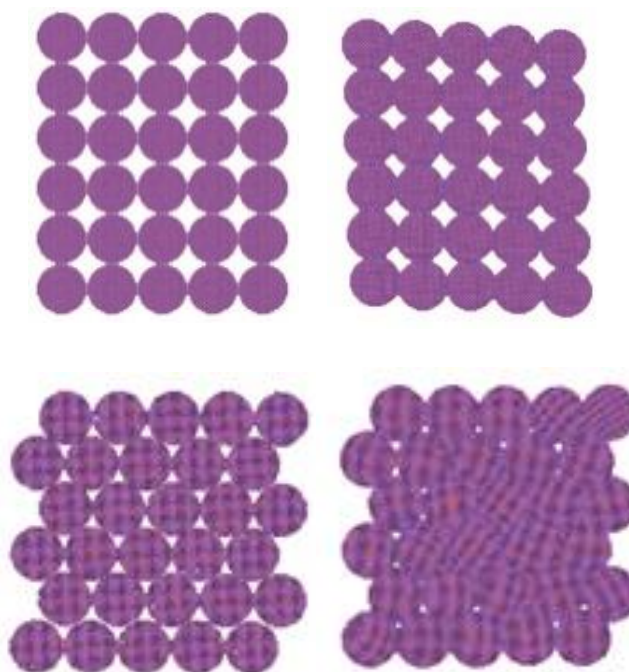
Figure 10: Type "A" and "C" Before and After Solid Sintering

As observed from the sintering illustrations, Type "C" NP stacking structures change more dramatically during the solid-state process. From the initial stage to the final duration of solid sintering, shrinkage is seen in both stacking types, however, in type "C", voids between particles almost completely enclose. Thus, this shows that there is higher fusion ability between type "C" particles than with the normal "type A" stack. This can also be observed in the relative radius of gyration (R_g^2) graphs in figure 2 where type "C" values drop more significantly from initial state than those of Type "A".
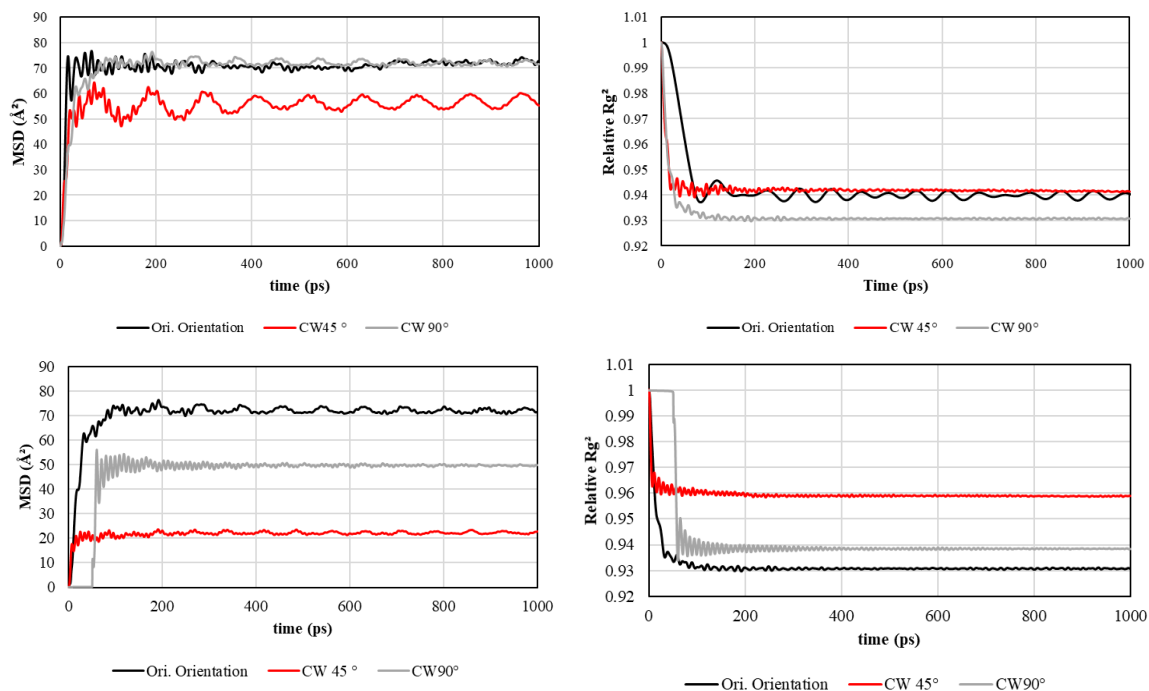
*Figure 11: Solid State Sintering (**top**) a.)MSD- Type A Particle Orientation Variance b.)Rg- Type A, Particle Orientation Variance (**bottom**) c.)MSD- Type C Particle Orientation Variance d.)Rg- Type C Particle Orientation Variance*

Particle orientation is also observed throughout the initial solid-state simulation. This variation is studied for both "A" and "C" type stacks. Values for shrinkage from original structure are shown for each case and displayed in table 1.

Table 1: Shrinkage Values for Solid Sintering Process

	Original Orientation	Clockwise 45°	Clockwise 90°
"A Type"	6.097%	5.860%	6.930%
"C Type"	6.930%	4.100%	6.160%

The resulting shrinking values show that shrinkage trends vary with changing particle orientation. For example, by rotating the normally oriented NP to the formation with 45° rotation in both "A" and "C" types, the common trend recognized is where "C" type atoms experience

more shrinkage is reversed. There is no common trend noticed between particle orientations, showing that while the orientation does invoke differences in solid sintering outcome, this effect is random.

Melting Process

Both stacking sequence patterns with all observed NP orientations were sintered with two heating rates: 0.2 K/ps and 0.5 K/ps. Melting temperatures are observed and recorded for all varying cases using the MSD graphs and images of phase change from the melting process. On each MSD graph, there is a point where MSD drastically increases within a narrow temperature range. This value on the plot can be referenced as the sequence's fusion point. MSD graphs for varying stacking types and heating rates are shown in figure 11 below.
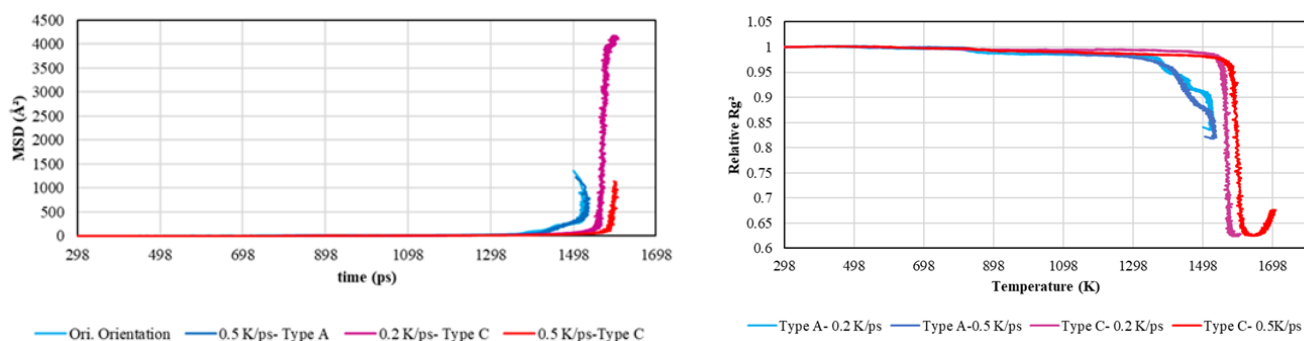
Figure 12: a.) MSD Plot Comparing Stacking Sequences b.) Radius of Gyration Plots Comparing Stacking Sequences
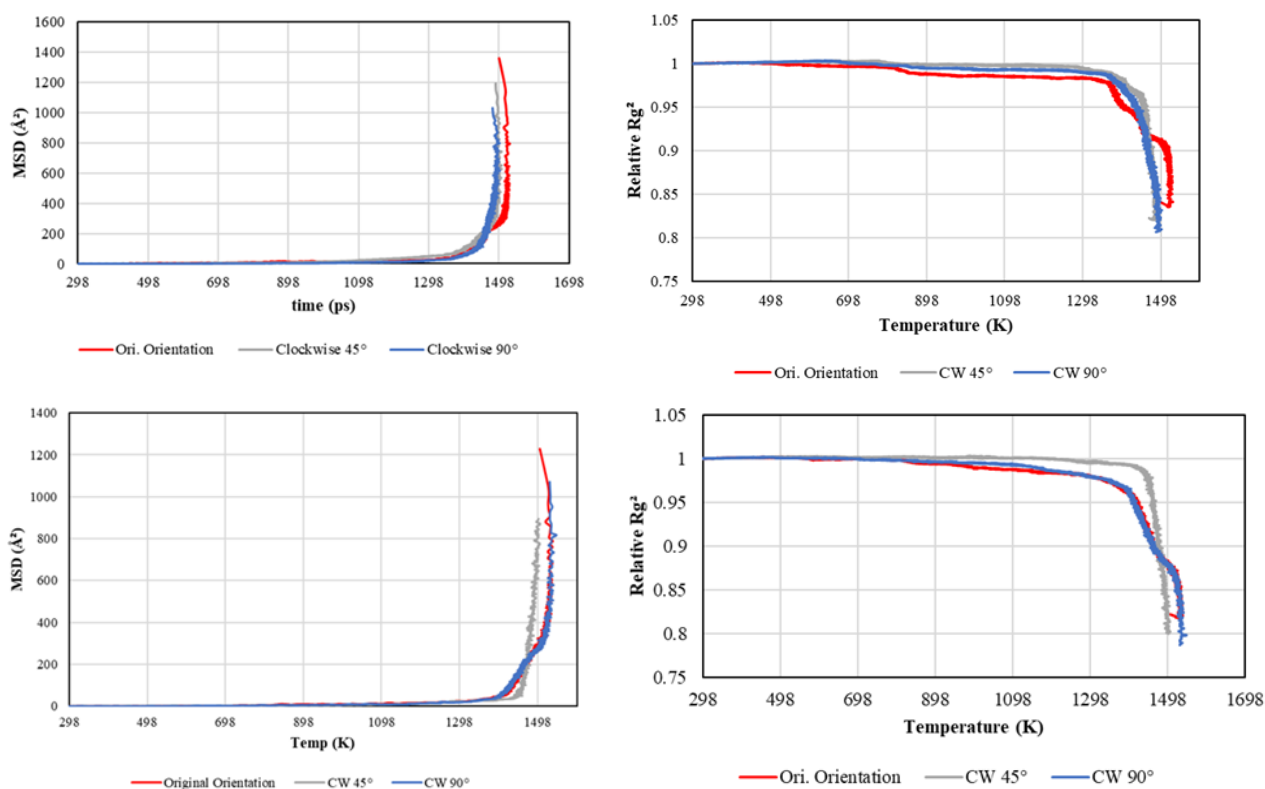
Figure 13: (left to right, top to bottom) a.)MSD- Type A, 0.2K/ps HR b.)Rg- Type A, 0.2K/ps HR c.)MSD-Type A, 0.5K/ps d.)Rg-Type A, 0.5 K/ps
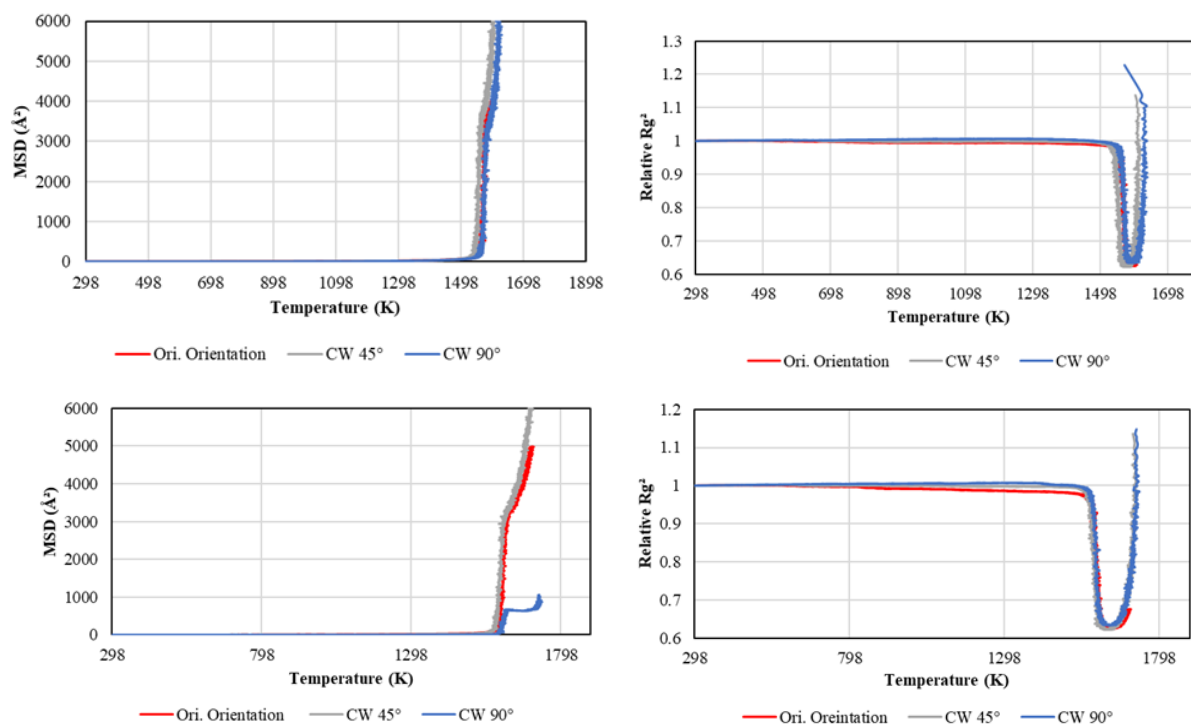
Figure 14:(left to right, top to bottom) a.)MSD- Type C, 0.2K/ps HR b.)Rg- Type C, 0.2K/ps HR c.)MSD-Type C, 0.5K/ps d.)Rg-Type C, 0.5 K/ps

This point signifies where the NP structures gain enough energy to liquify. Here, the particles in the NP stack begin to coalesce together. The temperature of sharp increase in which the particles join to fill all voids between particles is considered its melting point. Melting temperatures between cases are compared in Table 2. These values are taken from the MSD graph and confirmed with OVITO imaging throughout the melting process.

	Original Orientation	Clockwise 45°	Clockwise 90°
Type A- 0.2 K/ps HR	1459 K	1447 K	1456 K
Type A- 0.5 K/ps HR	1457 K	1480 K	1459 K
Type C- 0.2 K/ps HR	1545 K	1543 K	1562 K
Type C- 0.5 K/ps HR	1574 K	1567 K	1572 K

Table 2: Fusion Temperatures for Various Stacking Sequences

Comparing "type A" and "type C" molecules, there is a clear distinction between the melting behaviors of the two. "Type A" shows lower coalescence temperatures than "type C" in both heating rate cases. This has been attributed to the increased number of necks surrounding a single NP in the "C" stack as opposed to the "A" type. In the case of the "C type", every single NP has six surrounding neighbors, thus 6 necks surrounding each particle as opposed to only 4 in the "A type". Because of the increased number of connections and thus more surface area, it is believed that the type C stacking sequence is more stable than "type A", explaining the trend of increased melting temperatures. When comparing results from varying heating rates, there also shows to be an increase between the melting temperatures of the simulations heated with a 0.5 K/ps heating rate as opposed to those with a 0.2 K/ps heating rate in both stacking sequences.

The resulting variance in heating rate has a different effect when heating the stacking sequence as opposed to the single chain simulations. Typically, as seen in the 5-NP single chain simulations, a slower heating rate will yield a more stable heating process and thus higher melting temperatures. However, the heating simulations of the NP stacks seem to reverse this effect as the simulations with 0.5 K/ps heating rates have higher melting temperatures across all results. Lastly, when comparing heating temperatures between the varying particle orientations, the orientation seems to have an effect; however, with no identifiable trend. In the "type A" stacking sequence, rotating the particle 45° clockwise seems to be the orientation that has greatest effect on the melting behavior. In stacking sequence "C", there is no identifiable trend in melting behavior across cases.

Lastly, to observe the crystal structure of NP sequence through the laser sintering process, CNA graphs are used to identify any phase changes from solid sintered state to melting.

Ori orien.

Ori orien.
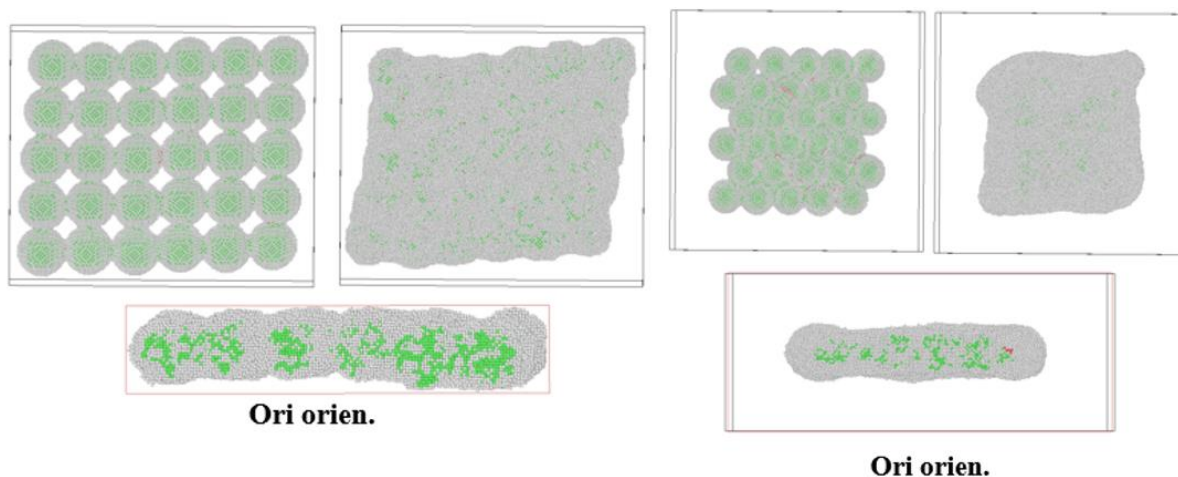
Figure 15: CNA Images for Final Sintered Product for Sequenced Structures

In both "A" and "C" type sequences, the initial predominantly present crystal type is FCC with disordered atoms on the outer perimeter of each nanoparticle. However, especially between the neck connections of each nanoparticle, there are a small percentage of HCP particles present after the initial solid sintering of each sequence type. As the sequence types are heated toward

melting levels, the fraction of disordered atoms begins to dominate. This is expected in heating toward melting temperatures as crystal lattices begin to slip past each other in phase transition. Thus, the crystal structure evolves to be disordered. This evolution of crystal structure in the heating process is shown in figure 15 using OVITO common neighbor analysis images.

CONCLUSION

From the resulting MD simulations of the SLS process of single chain and stacked γ-TiAl configurations, it is confirmed that in both the stacked and single chain formations, sintering temperature and rate will have a consistent effect on the final product. In the case of the single chain, higher sintering temperatures result in stronger neck connections between each individual NP as seen from the results from MSD and gyration radii results as well as the associated images. Additionally, in comparing the two products heated at 0.2 and 0.04 K/ps, it is observed that the slower heating rate results in an oscillating displacement with larger neck growth as seen from the results of the gyration radius and images. From the observation and comparison of common neighbor analysis images, the slower heating rates indicate a more thoroughly sintered product as the final stage of melting shows an increased number of disordered atoms. This implies a more unified phase change amongst atoms and thus, increased sintered quality. Finally because of this increased quality, it is found through tensile testing that the chains heated slowest and to highest temperatures are strongest and most ductile.

In the case of the stacking sequence, both sintering rate, particle orientation, and stacking type were varied and analyzed. Between the two stacking configurations, type "A" and type "C" were compared as they were heated to their respective melting temperatures at 0.2 and 0.5 K/ps. It is observed that stacking type has a definitive difference on the melting behavior of the stacking patterns. Overall, type "C" displayed higher melting temperatures than type "A". This is assumed to be caused by the fact that type "C" has an increased number of neck connections

leading to more surface area to sinter and more stable particle connections which will require an elevated temperature to cause the transition in phase change. Additionally, the particle configuration is seen to cause a difference in solid sintering and melting trends, however, they show no consistent trends. Thus, particle orientation has a random effect on sintered products as it would in real physical laser sintering scenarios. Sintering rate has an opposite effect on melting behavior in the case of stacked particles than in single chain simulations. In the case of single chain heating, slower heating rates usually yield higher melting temperatures as the slower heating is associated with a more stable melting process. However, in stacked sequences of particles, the stacks heated with 0.5 K/ps heating rate yield higher melting temperatures in both stacking pattern types.

Future work will be interested in the variation of strain rates in tensile simulations. As previously discussed, the issue concerning the erroneous MSD results with single chain sintering will also be addressed. Additionally, work could be conducted in the application of multidirectional stresses in the case of stacking sequence products.

BIBLIOGRAPHY:

[1] Kruth, J. P., Wang, X., Laoui, T., & Froyen, L. (2003, December 1). *Lasers and materials in Selective Laser Sintering*. Assembly Automation. Retrieved March 2, 2022, from https://www.emerald.com/insight/content/doi/10.1108/01445150310698652/full/html

[2] Hong, S. (2018). *(PDF) Selective Laser Sintering of nanoparticles*. Retrieved March 2, 2022, from https://www.researchgate.net/publication/322999173_Selective_Laser_Sintering_of_Nano particles

[3] Ding, L., Davidchack, R. L., & Pan, J. (2009). A molecular dynamics study of sintering between nanoparticles. *Computational Materials Science*, *45*(2), 247–256. https://doi.org/10.1016/j.commatsci.2008.09.021

[4] Wu, H. N., Xu, D. S., Wang, H., & Yang, R. (2016). Molecular dynamics simulation of tensile deformation and fracture of γ-tial with and without surface defects. *Journal of Materials Science & Technology*, *32*(10), 1033–1042. https://doi.org/10.1016/j.jmst.2015.12.001

[7] Jeon, J., Jiang, S., Rahmani, F., & Nouranian, S. (2020, January 9). *Molecular dynamics study of temperature and heating rate–dependent sintering of titanium nanoparticles and its influence on the sequent tension tests of the formed particle-chain products - Journal of Nanoparticle Research*. SpringerLink. Retrieved April 11, 2022, from https://link.springer.com/article/10.1007/s11051-019-4747-3

[6] Faken, D., & Jónsson, H. (1994). Systematic analysis of local atomic structure combined with 3D Computer Graphics. *Computational Materials Science*, *2*(2), 279–286. https://doi.org/10.1016/0927-0256(94)90109-0

[7] *LAMMPS documentation (24 Mar 2022 version)¶*. LAMMPS Documentation (24 Mar 2022 version) - LAMMPS documentation. (n.d.). Retrieved April 11, 2022, from https://docs.lammps.org/

[8] Jiang, S., Zhang, Y., Gan, Y., Chen, Z., & Peng, H. (2013). Molecular dynamics study of neck growth in laser sintering of hollow silver nanoparticles with different heating rates. *Journal of Physics D: Applied Physics*, *46*(33), 335302. https://doi.org/10.1088/0022-3727/46/33/335302

[9] Pan, Z., Li, Y., & Wei, Q. (2008). Tensile properties of nanocrystalline tantalum from molecular dynamics simulations. *Acta Materialia*, *56*(14), 3470–3480. https://doi.org/10.1016/j.actamat.2008.03.025

[10] Zhang, H., Jeon, J., Rahmani, F., Nouranian, S., & Jiang, S. (2021). Sintered ti/al core/shell nanoparticles: Computational investigation of the effects of core volume fraction, heating rate, and room-temperature relaxation on tensile properties. *Journal of Physics D: Applied Physics*, *55*(2), 025302. https://doi.org/10.1088/1361-6463/ac2ad7